

CrossMark  
click for updatesCite this: *J. Mater. Chem. A*, 2016, 4, 10014

# Uncovering the prominent role of metal ions in octahedral *versus* tetrahedral sites of cobalt–zinc oxide catalysts for efficient oxidation of water†

Prashanth W. Menezes,<sup>a</sup> Arindam Indra,<sup>a</sup> Arno Bergmann,<sup>b</sup> Petko Chernev,<sup>c</sup> Carsten Walter,<sup>a</sup> Holger Dau,<sup>\*c</sup> Peter Strasser<sup>\*b</sup> and Matthias Driess<sup>\*a</sup>

The fabrication and design of earth-abundant and high-performance catalysts for the oxygen evolution reaction (OER) are very crucial for the development and commercialization of sustainable energy conversion technologies. Although spinel catalysts have been widely explored for the electrochemical oxygen evolution reaction (OER), the role of two geometrical sites that influence their activities has not been well established so far. Here, we present more effective cobalt–zinc oxide catalysts for the OER than 'classical'  $\text{Co}_3\text{O}_4$ . Interestingly, the significantly higher catalytic activity of  $\text{ZnCo}_2\text{O}_4$  than that of  $\text{Co}_3\text{O}_4$  is somewhat surprising since both crystallize in the spinel-type structure. The reasons for the latter remarkable difference of  $\text{ZnCo}_2\text{O}_4$  and  $\text{Co}_3\text{O}_4$  could be deduced from structure–activity relationships of the bulk and near-surface of the catalysts using comprehensive electrochemical, microscopic and spectroscopic techniques with a special emphasis on the different roles of the coordination environment of metal ions (octahedral vs. tetrahedral sites) in the spinel lattice. The vital factors influencing the catalytic activity of  $\text{ZnCo}_2\text{O}_4$  over  $\text{Co}_3\text{O}_4$  could be directly attributed to the higher amount of accessible octahedral  $\text{Co}^{3+}$  sites induced by the preferential loss of zinc ions from the surface of the  $\text{ZnCo}_2\text{O}_4$  catalyst. The enhanced catalytic activity is accompanied by a larger density of metal vacancies, defective sites and hydroxylation. The results obtained here clearly demonstrate how a surface structural modification and generation of defects of catalysts can enhance their OER performance.

Received 1st May 2016  
Accepted 2nd June 2016

DOI: 10.1039/c6ta03644a

[www.rsc.org/MaterialsA](http://www.rsc.org/MaterialsA)

## Introduction

Water-splitting is an attractive alternative for renewable energy conversion and storage and plays a key role as a sustainable substitute for fossil fuels. In water splitting, hydrogen serving as a chemical storage molecule for renewable energy sources is generated in a clean way; however, the anodic oxygen evolution reaction (OER) requires multielectron transfer which leads to significant overpotential.<sup>1–6</sup> Therefore, presently, one of the main focuses is to prepare catalysts that can drive the OER very

efficiently.<sup>7–13</sup> Inspired by the natural photosystem (PS II), extensive investigations have been carried out in recent years to establish the most efficient catalytic systems.<sup>14–21</sup> The efforts have already been substantiated by various researchers, by synthesizing promising OER catalysts towards conversion of electrical energy into chemical energy.<sup>22–27</sup>

Noble metal based oxide materials such as  $\text{RuO}_2$  and  $\text{IrO}_2$  have been considered highly effective for the OER with lower overpotentials (the difference between the acquired potentials during the OER and the theoretical potential of the OER) and lower Tafel slopes (the slope of the linear part of the potential vs. the log of the current density)<sup>28–31</sup> while their scarcity and high cost are major drawbacks with respect to large-scale synthesis and practical applications.<sup>32–34</sup> In the meantime, several non-noble metal oxide OER catalysts have been discovered that are inexpensive and earth abundant. Special interest has been devoted to the first-row transition metals, particularly, spinel-type cobalt oxide based materials, as they not only show an efficient OER but are also applicable in oxygen reduction reactions (ORRs), and as anode materials in Li-ion batteries.<sup>35–38</sup> Although, over the years, numerous crystalline and amorphous cobalt oxides (Co) and substituted metal oxides based on cobalt (Co–Mn, Co–Fe, Co–Ni, and Co–Cu) have been widely

<sup>a</sup>Department of Chemistry, Metalorganics and Inorganic Materials, Technische Universität Berlin, Straße des 17 Juni 135, Sekr. C2, 10623 Berlin, Germany. E-mail: matthias.driess@tu-berlin.de

<sup>b</sup>Department of Chemistry, The Electrochemical Energy, Catalysis, and Materials Science Group, Technische Universität Berlin, Straße des 17 Juni 124, Sekr. TC3, 10623 Berlin, Germany. E-mail: pstrasser@tu-berlin.de

<sup>c</sup>Fachbereich Physik, Freie Universität Berlin, Arnimallee 14, 14195 Berlin, Germany. E-mail: holger.dau@fu-berlin.de

† Electronic supplementary information (ESI) available: Experimental and instrumental details; PXRD patterns; EDX spectra; ICP-AES analyses; IR spectra; crystal structures, SEM; TEM; XPS and XAS spectra of all plots concerning the electrochemical OER as well as the characterization after the electrochemical measurements. See DOI: 10.1039/c6ta03644a

investigated for efficient OER electrocatalysis,<sup>23,39–50</sup> the combination of cobalt and zinc oxide is still very limited and unexplored. Li *et al.* deposited  $\text{ZnCo}_2\text{O}_4$  on a nickel substrate by electrophoretic deposition (EPD) as an electrocatalyst for the OER<sup>51</sup> while Sun *et al.* fabricated  $\text{Zn}_x\text{Co}_{3-x}\text{O}_4$  nanoarrays on titanium foils for the same purpose.<sup>52</sup> In addition to this, we designed a self-supported cobalt doped zinc oxide catalyst (Co : ZnO) utilizing a molecular approach for unifying oxidant-driven OER and electrochemical OER, whereas Yang *et al.* reported cobalt zinc oxides for oxidant-driven water oxidation.<sup>53</sup> Similarly, Li *et al.* explored ZnCo-layered double hydroxide nanowalls toward efficient electrochemical water oxidation and recently, Choi *et al.* prepared plate-like  $\text{ZnCo}_2\text{O}_4$  and  $\text{CoCo}_2\text{O}_4$  *via* an electrochemical route and compared their OER activity, suggesting that tetrahedral sites are probably noncritical for the OER.<sup>54</sup> Even though the activity comparison between  $\text{ZnCo}_2\text{O}_4$  and  $\text{Co}_3\text{O}_4$  has been made, no surface structural investigations and structure–activity relationships have been derived so far. In this context, we directed ourselves to explore the cobalt zinc oxide system for OER catalysis and thoroughly investigate the impact of chemical surface characteristics, the role of metal ions in the spinels and structural influence on the activity.

Here, we present the large-scale synthesis of cobalt–zinc oxides that were further examined for the electrochemical OER in alkaline solution. The performance of spinel  $\text{ZnCo}_2\text{O}_4$  was significantly higher than that of  $\text{Co}_3\text{O}_4$  while  $(\text{Co}_3\text{O}_4)/(\text{ZnO})_6$  showed limited activity and ZnO was proved to be inactive. All catalysts were investigated in depth using microscopic and spectroscopic techniques before and after the OER to identify structural and morphological changes induced by the electrocatalytic reaction. The pivotal factors associated with the higher activity of  $\text{ZnCo}_2\text{O}_4$  over  $\text{Co}_3\text{O}_4$  can be ascribed to the higher amount of accessible Co sites and formation of cationic vacancies due to the preferential loss of zinc ions from the near-surface of the  $\text{ZnCo}_2\text{O}_4$  catalyst during the OER. The results obtained here not only demonstrate the synthesis of high performance catalysts by a scalable route but also evidence the influence of the near-surface structure on the activity, which could be very useful in designing economic and active OER catalysts.

## Results and discussion

$\text{ZnCo}_2\text{O}_4$ ,  $(\text{Co}_3\text{O}_4)/(\text{ZnO})_6$ , ZnO, and  $\text{Co}_3\text{O}_4$  were synthesized by annealing their respective hydroxide carbonate precursors (see ESI†) and comprehensively characterized (Fig. S1–S5, and Tables S1 and S2†). The oxide phases were first examined by Powder X-Ray Diffraction (PXRD) that indeed suggested the phase purity of the as-synthesized products (Fig. S6†). The reflections obtained by PXRD could be well assigned to the crystalline  $\text{ZnCo}_2\text{O}_4$  (JCPDS 23-1390),  $(\text{Co}_3\text{O}_4)/(\text{ZnO})_6$  (JCPDS 42-1467 and 75-576), ZnO (JCPDS 75-576), and  $\text{Co}_3\text{O}_4$  (JCPDS 42-1467).  $\text{ZnCo}_2\text{O}_4$  and  $\text{Co}_3\text{O}_4$  crystallize in the cubic system with space group  $Fd\bar{3}m$  (Nr 227) and have a spinel structure ( $\text{A}^{2+}\text{B}_2^{3+}\text{O}_4$ , where A is the tetrahedral site and B is the octahedral site).<sup>55,56</sup> ZnO belongs to the hexagonal wurtzite system with space group  $P6_3mc$  (No. 186) where both zinc and oxygen are in

tetrahedral coordination (Fig. S7†).<sup>57</sup> The chemical composition (Co/Zn ratio) of  $\text{ZnCo}_2\text{O}_4$  and  $(\text{Co}_3\text{O}_4)/(\text{ZnO})_6$  was also determined by Inductively Coupled Plasma Atomic Emission Spectroscopy (ICP-AES) that was in accordance with the ratio obtained from the precursor and derived chemical formulae (Table S1†). The morphology and the detailed structure of the as-synthesized oxides were provided by Scanning Electron Microscopy (SEM) and Transmission Electron Microscopy (TEM). Both SEM (Fig. S8†) and TEM (Fig. S9†) images displayed that  $\text{ZnCo}_2\text{O}_4$  forms nanochains, whereas nanofibrous type morphology built of nanoparticles was procured for  $(\text{Co}_3\text{O}_4)/(\text{ZnO})_6$ . In contrast, ZnO was comprised of nanonets while spherical shaped particles were accessible for  $\text{Co}_3\text{O}_4$  (Fig. 1). The difference in the morphology of  $\text{ZnCo}_2\text{O}_4$  and  $\text{Co}_3\text{O}_4$  could be explained by the difference in the nucleation and growth mechanism due to two different ions involved in the process. Further, the reflections from the Selected-Area Electron Diffraction (SAED) pattern, extracted from High-Resolution TEM (HR-TEM) images, additionally confirmed the phase identification (Fig. S10†). In addition, it could distinctly be seen that  $\text{Co}_3\text{O}_4$  was well embedded dispersed in the ZnO matrix to form  $(\text{Co}_3\text{O}_4)/(\text{ZnO})_6$  (Fig. S10†). Interestingly, the Brunauer–Emmett–Teller (BET) surface area of  $\text{ZnCo}_2\text{O}_4$  was found to be higher ( $57 \text{ m}^2 \text{ g}^{-1}$ ) than that of  $(\text{Co}_3\text{O}_4)/(\text{ZnO})_6$  ( $42.9 \text{ m}^2 \text{ g}^{-1}$ ), ZnO ( $30.3 \text{ m}^2 \text{ g}^{-1}$ ) and  $\text{Co}_3\text{O}_4$  ( $38.1 \text{ m}^2 \text{ g}^{-1}$ ).

The detailed chemical bonding states of Co(III), Co(II,III) and Zn(II) for the as-synthesized oxides were further analyzed by X-ray Photoelectron Spectroscopy (XPS). From the literature, it is already known that for Co2p XPS, the Co(II) and Co(III) have almost similar 2p binding energies (BE) but they can be differentiated by the  $\text{Co}2p_{1/2}-2p_{3/2}$  spin–orbit level energy spacing, which is 16.0 eV for high-spin Co(II) and 15.0 eV for low-spin Co(III).<sup>58</sup> The BEs of Co in  $\text{ZnCo}_2\text{O}_4$  were found to be

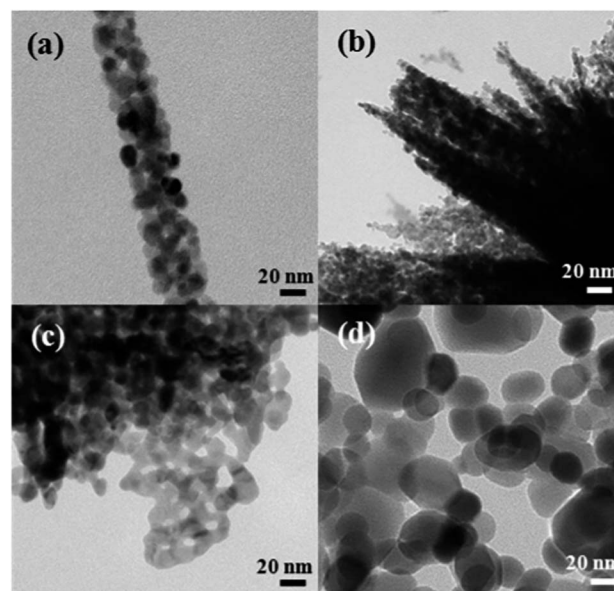


Fig. 1 TEM images of (a) nanochains of  $\text{ZnCo}_2\text{O}_4$ , (b) nanofibrous structures of  $(\text{Co}_3\text{O}_4)/(\text{ZnO})_6$ , (c) nanonets of ZnO and (d) spherical shaped  $\text{Co}_3\text{O}_4$  particles (see additional images in Fig. S9 and S10†).

794.7 eV for  $\text{Co}2p_{1/2}$  and 779.7 eV for  $\text{Co}2p_{3/2}$  with a difference of 15 eV, and are consistent with values of  $\text{Co(III)}$ , whereas BEs of Co in  $(\text{Co}_3\text{O}_4)/(\text{ZnO})_6$  and  $\text{Co}_3\text{O}_4$  (Fig. 2) were very similar and close to  $\sim 795.8$  eV for  $\text{Co}2p_{1/2}$  and  $\sim 780.2$  eV for  $\text{Co}2p_{3/2}$  confirming  $\text{Co(II,III)}$ .<sup>59</sup> The Zn2p spectra (Fig. S11†) display two peaks with BE values of  $\sim 1022.6$  and  $\sim 1044.9$  eV, which are ascribed to  $\text{Zn}2p_{3/2}$  and  $\text{Zn}2p_{1/2}$ , indicating the oxidation state of  $\text{Zn(II)}$ .<sup>60,61</sup> In addition, the Zn : Co ratio was also consistent with 1 : 2 and 2 : 1 for  $\text{ZnCo}_2\text{O}_4$  and  $(\text{Co}_3\text{O}_4)/(\text{ZnO})_6$ . The O1s spectrum (Fig. S12†), in each case, was deconvoluted into three peaks (O1, O2 and O3) corresponding to metal–oxygen bonds of metal oxide (O1), –OH groups (O2) and adsorbed water molecules (O3) on the materials. The values obtained in all cases could also be well matched with the other literature reported oxide materials.<sup>62–64</sup>

Electrocatalytic OER activity was examined using a rotating disk electrode (RDE) experiment. Fig. S13† shows the linear sweep voltammograms of  $\text{ZnCo}_2\text{O}_4$ ,  $(\text{Co}_3\text{O}_4)/(\text{ZnO})_6$ , ZnO and  $\text{Co}_3\text{O}_4$  recorded in  $\text{N}_2$ -saturated 0.1 M KOH solution.  $\text{ZnCo}_2\text{O}_4$  and  $\text{Co}_3\text{O}_4$  show a similar onset potential but at a current density of  $21 \text{ mA cm}^{-2}$ ;  $\text{ZnCo}_2\text{O}_4$  exhibits a lower electrode potential of 1.66 V compared to 1.70 V for the  $\text{Co}_3\text{O}_4$ . The  $(\text{Co}_3\text{O}_4)/(\text{ZnO})_6$  electrode was less active than  $\text{Co}_3\text{O}_4$  exhibiting a current density of  $17.5 \text{ mA cm}^{-2}$  at 1.88 V while ZnO was inactive for the OER. This shows that the  $\text{ZnCo}_2\text{O}_4$  shows an enhanced OER mass-activity at technologically feasible current densities compared to  $\text{Co}_3\text{O}_4$  and  $(\text{Co}_3\text{O}_4)/(\text{ZnO})_6$ . Remarkably, at  $20 \text{ mA cm}^{-2}$ , the overpotential displayed here was only 420 mV for  $\text{ZnCo}_2\text{O}_4$  and 460 mV for  $\text{Co}_3\text{O}_4$  that surpasses that of many of the active cobalt catalysts.<sup>45,54,65–68</sup> Interestingly, the results displayed here for  $\text{ZnCo}_2\text{O}_4$  not only show the importance of zinc in the spinel structure (see the discussion later on) but also show that this catalyst could enter as a potential non-precious candidate for benchmarking of systems, recently published by Jaramillo *et al.*<sup>69,70</sup>

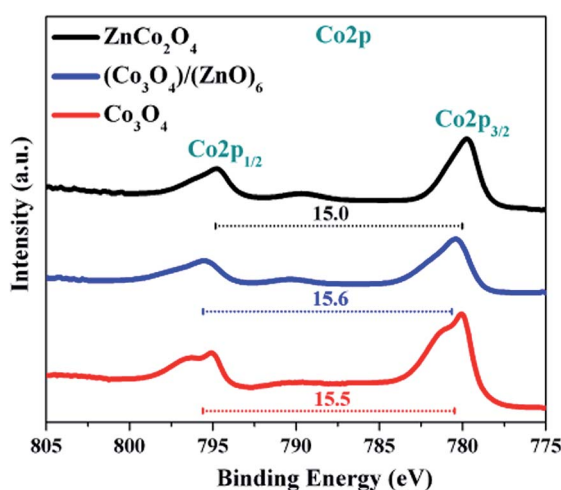


Fig. 2 The Co2p XPS spectra of  $\text{ZnCo}_2\text{O}_4$ ,  $(\text{Co}_3\text{O}_4)/(\text{ZnO})_6$  and  $\text{Co}_3\text{O}_4$ . The  $\text{Co(II)}$  and  $\text{Co(III)}$  have almost similar 2p binding energies but they can be differentiated by the  $\text{Co}2p_{1/2}$ – $2p_{3/2}$  spin–orbit level energy spacing, which is 16.0 eV for high-spin  $\text{Co(II)}$  and 15.0 eV for low-spin  $\text{Co(III)}$ , and are consistent with literature reported spinel oxides.

To investigate differences in the electrochemical surface area and the metal oxide redox chemistry, cyclic voltammograms (CVs) were recorded in 0.1 M KOH (Fig. 3).<sup>52,71</sup> The first pair of redox peaks (I/II) between 1.2 and 1.3 V corresponds to  $\text{Co}^{2+}/\text{Co}^{3+}$ , and was similar for both  $\text{ZnCo}_2\text{O}_4$  and  $\text{Co}_3\text{O}_4$ . Although the first redox peaks were not clearly visible, they were described in accordance to the known Co–Zn oxides.<sup>52</sup> However, the next pair of redox peaks (III/IV) in the range of 1.3 to 1.6 V, associated with  $\text{Co}^{3+}/\text{Co}^{4+}$ , displayed a notable variation.<sup>72–74</sup> The  $\text{ZnCo}_2\text{O}_4$  exhibited a substantially larger redox charge compared to  $\text{Co}_3\text{O}_4$ . This illustrates that a higher number of redox active  $\text{Co}^{3+}$  ions were available for  $\text{ZnCo}_2\text{O}_4$ . Further, for  $(\text{Co}_3\text{O}_4)/(\text{ZnO})_6$ , the redox charge was significantly lower which can be explained by a potential blocking of Co sites in the ZnO matrix.

The electrocatalytic properties of OER processes are attainable by approximating Tafel slopes and were extracted from quasi-stationary conditions in the potential range of 1.45–1.75 V (Fig. 4). A Tafel slope of  $58.6 \text{ mV dec}^{-1}$  was determined for  $(\text{Co}_3\text{O}_4)/(\text{ZnO})_6$ , whereas a value of  $40.5 \text{ mV dec}^{-1}$  was identified for  $\text{Co}_3\text{O}_4$ . The Tafel slope is even lower for  $\text{ZnCo}_2\text{O}_4$  ( $38.5 \text{ mV dec}^{-1}$ ) demonstrating more efficient reaction kinetics for oxygen evolution.<sup>23,75,76</sup> The Tafel values displayed for  $\text{ZnCo}_2\text{O}_4$  are among the lowest values reported in the literature for the transition metal oxide based catalysts and the best among the cobalt–zinc based catalysts.<sup>52,54,69,70,77–79</sup>

We performed the normalization of the catalytic current to the total redox charge as cyclic voltammograms were recorded at increased sweep rates between 1.0 V and  $\sim 1.58$  V. Under these conditions, the capacitive current and the current from the redox transitions are significantly higher than the catalytic current. We chose this method because we could use the same electrode for surface determination and catalytic testing without using metal additives that could have secondary effects such as Fe-incorporation and could have severe influence on the electrochemical and electrocatalytic properties. Interestingly, the catalytic activity normalized to the electrochemically

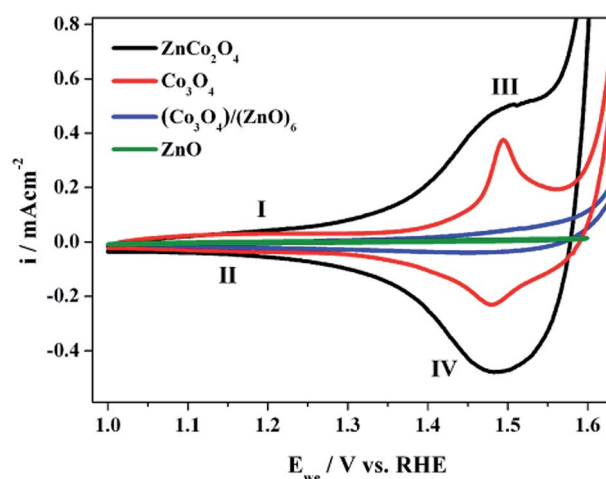


Fig. 3 Cyclic voltammograms of  $\text{ZnCo}_2\text{O}_4$ ,  $(\text{Co}_3\text{O}_4)/(\text{ZnO})_6$ , ZnO, and  $\text{Co}_3\text{O}_4$  electrodes recorded at a potential sweep rate of  $50 \text{ mV s}^{-1}$  at 1600 rpm in  $\text{N}_2$ -saturated 0.1 M KOH solution.



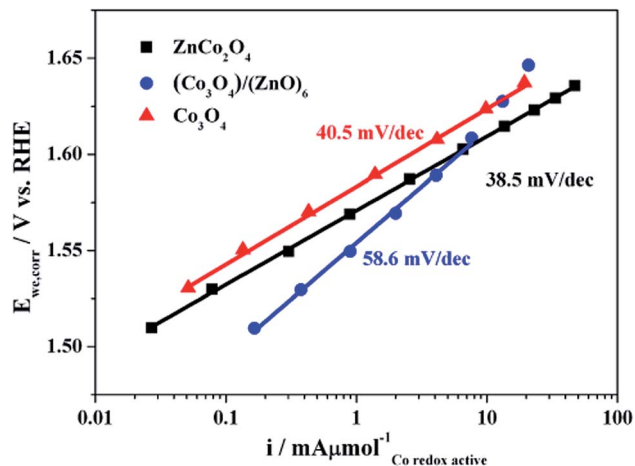


Fig. 4 Tafel plot of  $\text{ZnCo}_2\text{O}_4$ ,  $(\text{Co}_3\text{O}_4)/(\text{ZnO})_6$  and  $\text{Co}_3\text{O}_4$  extracted from quasi-stationary potential-step conditions ( $5 \text{ min}/E_{\text{step}}$ ) in  $0.1 \text{ M KOH}$  solution. Current was normalized to the number of redox active Co ions  $N$  as determined from the total reductive charge  $q$  of the CV recorded with  $50 \text{ mV s}^{-1}$  (see Fig. 3) by using  $N = q/F$  with  $F = 96485 \text{ C mol}^{-1}$ . The quasi-stationary potential step experiments were performed after initial activation by two CV ( $6 \text{ mV s}^{-1}$ ) covering the OER range (see Fig. S13†).

accessible Co ions differed between the  $\text{ZnCo}_2\text{O}_4$  and the bare  $\text{Co}_3\text{O}_4$ . Thus, it is possible that the structural and compositional differences in the near-surface induced by Zn incorporation led to a higher specific OER activity.

One of the remarkable structural features of  $\text{ZnCo}_2\text{O}_4$  is that it forms a regular spinel structure where  $\text{Zn}^{2+}$  sites are only occupied by tetrahedral ( $T_d$ ) sites leaving  $\text{Co}^{3+}$  in octahedral ( $O_h$ ) sites. In contrast, the substituted (Mn, Fe, Ni, Cu *etc.*) cobalt oxide spinels have variable oxidation states and could occupy in both  $T_d$  and  $O_h$  sites. Due to the invariable coordination spheres and oxidation state of Zn, it is possible to compare  $\text{ZnCo}_2\text{O}_4$  to  $\text{Co}_3\text{O}_4$  and establish a structure–activity relationship. Previously, it has been discovered that in  $\text{Co}_3\text{O}_4$  (spinel type), the surface  $O_h \text{ Co}^{3+}$  sites are the actual active sites for the OER and the  $T_d \text{ Co}^{2+}$  sites are not catalytically active, and in fact, the trend has also been extended for the substituted cobalt oxides.<sup>37</sup> In addition to this, X-ray absorption analysis has also suggested that  $O_h \text{ Co}^{3+}$  sites are indeed the real active sites for the OER.<sup>37,80–82</sup> Nocera, Bell, Sun, and others delineated that, in cobalt based materials, prior to the OER, the  $O_h \text{ Co}^{3+}$  forms  $\text{Co}^{4+}$  species and enhances the electrophilicity of the adsorbed O and hence assists the formation of  $\text{O}-\text{OH}$  by nucleophilic attack and facilitates the deprotonation of  $-\text{OOH}$  through the electron-withdrawing inductive effect by forming oxygen.<sup>83–85</sup> Interestingly, in the crystal structure of  $\text{ZnCo}_2\text{O}_4$ , the  $T_d$  position is occupied only by  $\text{Zn}^{2+}$ , which in particular increases the  $\text{Co}^{3+}-\text{O}$  distance.<sup>52,61</sup> As described before, the greater the number of electrochemically accessible  $O_h \text{ Co}^{3+}$  sites, the higher the chances of  $-\text{OH}$  adsorption onto the  $\text{Co}^{3+}$  and therefore, a larger number of  $\text{Co}^{4+}$  species formed prior to the OER (see Fig. 3).

It is not sufficient to deduce a structure–activity relationship based only on the crystal structure and OER activity but rather should be concluded with surface structure phenomena that

transpire during the OER. To uncover this, chronoamperometry responses (Fig. S14†) of  $\text{ZnCo}_2\text{O}_4$ ,  $(\text{Co}_3\text{O}_4)/(\text{ZnO})_6$ ,  $\text{ZnO}$ , and  $\text{Co}_3\text{O}_4$  were also recorded at  $1.8 \text{ V vs. RHE}$  in  $0.1 \text{ M KOH}$  solution with  $1600 \text{ rpm}$  for the first  $30 \text{ min}$  and successive surface structure changes occurring during the OER were systematically studied. Although the current values for  $\text{ZnCo}_2\text{O}_4$  and  $\text{Co}_3\text{O}_4$  were maintained, a slight decrease in current was unveiled for  $(\text{Co}_3\text{O}_4)/(\text{ZnO})_6$  and as expected,  $\text{ZnO}$  was found to be inactive.

To identify the structural and compositional changes of the bulk and near-surface, all electrodes were further characterized by TEM, HRTEM, SAED, FT-IR and XPS before and after electrocatalysis. The TEM images and SAED pattern of all electrodes showed that the morphology and the crystallinity of the materials are well preserved after electrocatalysis (Fig. S15†). HRTEM images of  $\text{ZnCo}_2\text{O}_4$ ,  $(\text{Co}_3\text{O}_4)/(\text{ZnO})_6$  and  $\text{ZnO}$  revealed that the surfaces of the catalysts were slightly affected and appeared to be corroded (Fig. 5).

To elucidate the changes in the chemistry and composition of the near-surface, we carried out XPS on all catalysts after electrocatalysis. In  $\text{Co}2\text{p}$  XPS of  $\text{ZnCo}_2\text{O}_4$ ,  $(\text{Co}_3\text{O}_4)/(\text{ZnO})_6$  and  $\text{Co}_3\text{O}_4$ , the BEs were  $\sim 794.5 \text{ eV}$  for  $\text{Co}2\text{p}_{1/2}$  and  $\sim 779.5 \text{ eV}$  for  $\text{Co}2\text{p}_{3/2}$  with a spin–orbit level energy spacing difference of  $15 \text{ eV}$ , indicating that the higher fraction of  $\text{Co(III)}$  is available in the near-surface of the materials (Fig. 6).<sup>58</sup> Additionally, by deconvoluting and integrating the areas of  $\text{Co}^{3+}$  and  $\text{Co}^{2+}$ , taking out their  $\text{Co}^{3+}/\text{Co}^{2+}$  ratios, and comparing them with those of the as-prepared oxides, it was certain that the ratios of  $\text{Co}^{3+}/\text{Co}^{2+}$  were significantly increased ( $0.21$  to  $0.38$  for  $(\text{Co}_3\text{O}_4)/(\text{ZnO})_6$  and  $0.19$  to  $0.22$  for  $\text{Co}_3\text{O}_4$ ). However, in the case of  $\text{ZnCo}_2\text{O}_4$ ,  $\sim 30\%$  of Zn was lost from the near-surface. As anticipated,  $\text{Zn}2\text{p}$  XPS displayed two peaks (Fig. S16†) with BE values of  $\sim 1020.6$  and  $\sim 1043.5 \text{ eV}$ , which correspond to  $\text{Zn}2\text{p}_{3/2}$  and  $\text{Zn}2\text{p}_{1/2}$  and are

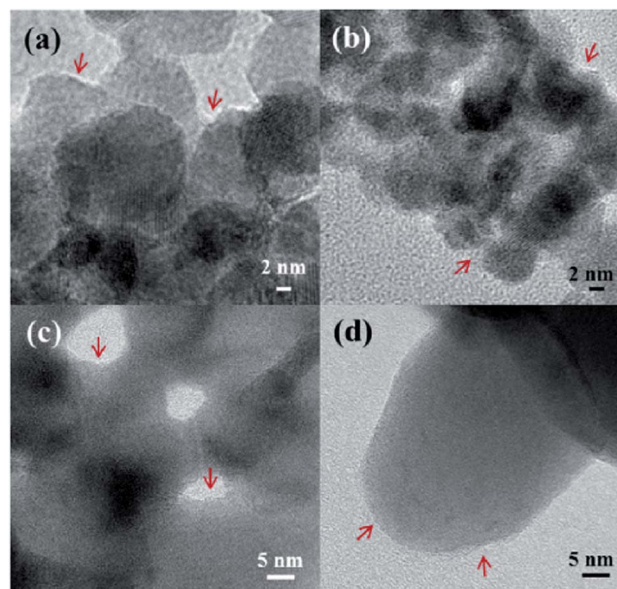


Fig. 5 HRTEM images of (a)  $\text{ZnCo}_2\text{O}_4$ , (b)  $(\text{Co}_3\text{O}_4)/(\text{ZnO})_6$ , (c)  $\text{ZnO}$ , and (d)  $\text{Co}_3\text{O}_4$  after chronoamperometry experiments. The red arrow indicates that the surface of the catalysts was affected but preserving their morphology and crystallinity (see also Fig. S15†).

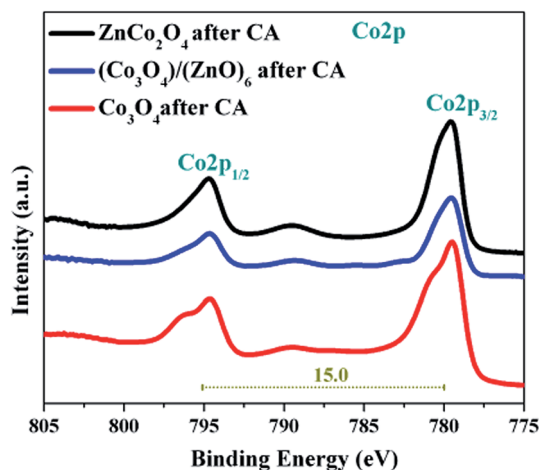


Fig. 6 The Co2p XPS spectra of  $\text{ZnCo}_2\text{O}_4$ ,  $(\text{Co}_3\text{O}_4)/(\text{ZnO})_6$  and  $\text{Co}_3\text{O}_4$  after chronoamperometry (CA) experiments. In all cases, the  $\text{Co}2p_{1/2}$ – $\text{Co}2p_{3/2}$  spin–orbit level energy spacing difference was found to be 15 eV and is consistent with values of  $\text{Co}(\text{III})$ .

consistent with the presence of  $\text{Zn}(\text{II})$ .<sup>60,61</sup> The O1s spectra showed dramatic changes between  $\sim 530.8$  and  $532.5$  eV in the O2 region (Fig. S17†). A higher fraction of  $-\text{OH}$  groups in the O2 region indicates that the near-surface of the material is largely hydroxylated.<sup>9,46</sup> The FT-IR spectra of the  $\text{ZnCo}_2\text{O}_4$  also showed a higher amount of hydroxylation when compared to the as-prepared catalyst (Fig. S18†). In addition to this, plotting catalytic activity vs. the percentage of hydroxylation clearly showed that the increasing hydroxylation is indeed beneficial for lowering the Tafel slopes (Fig. S19†).

As it was evident that  $T_d \text{Zn}^{2+}$  in  $\text{ZnCo}_2\text{O}_4$  leaches into the solution during the OER, the structural changes at the atomic scale were further studied by X-ray Absorption Spectroscopy (XAS) at the Co and Zn K-edge. First of all, the oxidation state and site symmetry were acquired from the X-ray Absorption Near Edge Structure (XANES), whereas the local structural details were deduced from the Extended X-ray Absorption Fine Structure (EXAFS) regions above the edge originating from the interference of the outgoing and backscattered photoelectron waves (see ESI† for details). The insets of Fig. 7 display the Co edge and Zn edge XANES spectra of  $\text{ZnCo}_2\text{O}_4$  before and after the OER (after chronoamperometry).

The mean oxidation state of the cobalt was estimated by the edge positions exhibited in the Co edge XANES spectrum. From the edge rise at 7721.4 eV, the average oxidation state of cobalt was estimated to be +3 (before and after the OER)<sup>50,86,87</sup> and the shape of the spectrum also clearly indicated the existence of a spinel type structure.<sup>50</sup> Although a slight change in the Zn edge XANES was visible (due to the loss of Zn from the near-surface), the edge at 9661.2 eV signified the presence of zinc in the mean oxidation state of +2.<sup>88,89</sup> On the other hand, the X-Ray Fluorescence Emission Spectra (XRF) showed a lower Zn fluorescence intensity for the sample after the OER, in comparison to the as-prepared  $\text{ZnCo}_2\text{O}_4$  (Fig. S20†). The difference in the intensity further evidences that around 25% of the zinc leaches

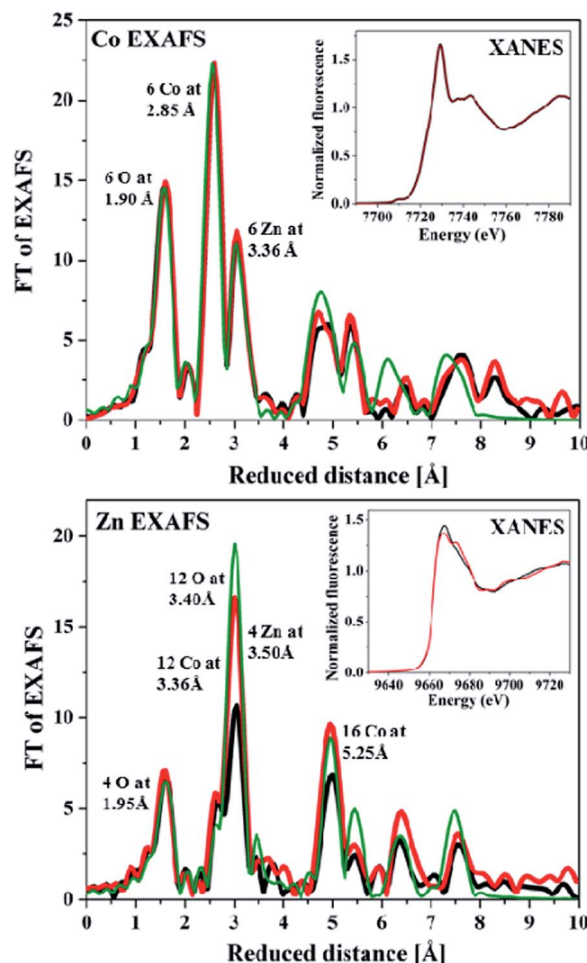


Fig. 7 The X-ray absorption spectra of  $\text{ZnCo}_2\text{O}_4$  deposited on electrodes. The insets show the Co and Zn edge regions of the spectra (XANES) before (black) and after (red) catalysis. Each peak in the Fourier-transformed EXAFS spectra relates to a specific structural motif and corresponding reduced distances are shown. The spectra obtained by EXAFS simulations for a perfect Co in octahedral sites of a spinel structure and Zn in tetrahedral sites are shown as green lines (simulation parameters are given in Table S4† and the structural fragments are shown in Fig. S22†), whereas the spectra of  $\text{ZnCo}_2\text{O}_4$  before and after catalysis are shown in black and red lines, respectively.

into the basic solution (as evidenced by ICP-AES, HRTEM, and XPS) under OER conditions.

In the Fourier transform (FT) Co EXAFS (Fig. 7) of  $\text{ZnCo}_2\text{O}_4$ , films both as-prepared and after the OER showed peaks at the lowest interatomic distance of 1.90 Å (additional EXAFS data and simulations are shown in Fig. S21 and Table S4†) and could be assigned to the Co–O bonds of  $O_h$  motif ( $\text{Co}^{3+}\text{O}_6$ ).<sup>90,91</sup> The next prominent FT peak corresponds to 6 Co–Co interactions at a distance of 2.85 Å and is typical for di- $\mu$ -oxido bridges (cobalt oxido cubanes and incomplete cubanes of the layer, see Fig. S22†). The FT peak at  $\sim 3$  Å is assigned to 6 Co–Zn, *i.e.*, linking between  $O_h \text{Co}^{3+}$  and  $T_d \text{Zn}^{2+}$  with a distance of 3.36 Å. The assignments of the first three FT peaks can be directly corroborated by EXAFS spectra of other cobalt oxide materials and, together with the peaks at higher distances, are consistent with cobalt in  $O_h$  sites of a spinel structure.<sup>86,91</sup>

Similarly, in the FT Zn EXAFS of  $\text{ZnCo}_2\text{O}_4$ , the first distance at 1.95 Å is consistent for Zn–O bonds for  $T_d$   $\text{Zn}^{2+}$  while the distances at 3.36 Å, 3.40 Å, and 3.50 Å could be well matched with 12 Zn–Co, 12 Zn–O and 4 Zn–Zn interatomic distances, respectively.<sup>53</sup> Furthermore, the FT peak corresponding to a distance of 5.25 Å is also representative for 16 Zn–Co distances in a material containing  $T_d$   $\text{Zn}^{2+}$  sites of a spinel. Interestingly, in the as-prepared sample, all FT peaks except the first Zn–O peak have lower amplitudes, which might be explained by the higher proportion of Zn in the as-prepared sample which is lost from the near-surface during OER treatment, leaving only well-ordered Zn in  $T_d$  sites in the particle core. From the XANES, XRF and EXAFS, it was certain that the  $O_h$   $\text{Co}^{3+}$  was not irreversibly affected during the OER process but the  $T_d$   $\text{Zn}^{2+}$  was lost from the near-surface most likely creating vacancies or defective sites at  $T_d$  or possible near-surface restructuring leading to hydroxylation. As known in the literature, for cobalt oxides, the  $O_h$   $\text{Co}^{3+}$  sites are the responsible active sites for the OER and our investigation further reveals that along with the  $O_h$   $\text{Co}^{3+}$  there could be additional vacancies or hydroxylation present in the near-surface due to the loss of  $T_d$   $\text{Zn}^{2+}$  during the OER.

The EXAFS data collected for the  $\text{ZnCo}_2\text{O}_4$ -type materials indicate the presence of a well-ordered spinel-type structure both before and after exposure to catalytic potentials. The agreement between the EXAFS spectra calculated for perfect crystallographic order and the experimentally detected spectra excludes any sizeable amorphization as a reason for superior activity in the Zn–Co spinel catalyst. The XPS data and the decreased Zn : Co stoichiometry – as clearly visible in the X-ray emission spectra (Fig. S20†) – evidence a clear loss of Zn ions from  $T_d$  sites. The O1s XPS data suggest that the loss of Zn ions is associated with the charge-compensating protonation of bridging oxides ( $\mu\text{-OH}$  formation). The vacancies resulting from Zn loss in conjunction with  $\mu\text{-OH}$  formation and likely also binding of terminally coordinated water species allow for redox-state changes by charge-neutral proton-coupled electron transfer as evidenced by the cyclic voltammograms in Fig. 3, where the magnitude of the redox features appears to correlate with OER activity. In conclusion, vacancy formation at the tetrahedral spinel sites facilitates redox-state changes and formation of active sites which comprise  $\text{Co(IV)}$  ions as well as coordination sites for the ‘substrate water’ of the OER in the  $\text{ZnCo}_2\text{O}_4$ -spinel material. Similarly also in the  $\text{Co}_3\text{O}_4$ -spinel material, the OER activity may result from a more limited release of cobalt ions from tetrahedral coordination sites.

Evaluating our extended investigation, the higher catalytic OER performance of  $\text{ZnCo}_2\text{O}_4$  in contrast to that of  $\text{Co}_3\text{O}_4$  can therefore be rationalized by the following aspects. First of all, substituting  $T_d$   $\text{Zn}^{2+}$  into the lattice of cobalt oxide results in nanochain morphology with a larger surface area (almost 1.5 times) thereby increasing accessible surfaces for the OER. Secondly, dissolution of Zn ions under OER conditions forms cationic vacancies at the surface which leads to a higher fraction of hydroxylation and defects in the near-surface lead to changes in the coordinative environment of the Co ions and are thought to significantly enhance the OER catalysis. Additionally, an additional activity-determining property of the electrocatalysts

must be present. If the difference in catalytic activity is only due to the (electrochemical) surface area then the normalization by using the number of redox active Co ions would eliminate this reason. However, it is not shown yet whether all redox active Co ions are also catalytically active. Therefore, this normalization does not necessarily lead to an identical specific OER activity. The effect of different specific OER activities has been already seen for other Ir-based catalysts.<sup>92,93</sup> Assuming that all redox active Co ions are also catalytically active, it leads to the point that the onset potential of the OER might differ. This difference can be related to the thermodynamics of Co redox transition and thus, to the strength of the Co–O bonds. Nevertheless, these differences are all related to the Zn dissolution, which leads to a structurally different and catalytically more active near-surface region of the  $\text{CoO}_x$  on the  $\text{Co}_2\text{ZnO}_4$  compared to that of  $\text{Co}_3\text{O}_4$ . It has recently been shown that at elevated OER, the near-surface of crystalline  $\text{Co}_3\text{O}_4$  transforms reversibly, and an amorphous, sub-nanometer shell of  $\text{CoO}_x(\text{OH})_y$  consisting of predominantly di- $\mu$ -oxo bridged  $\text{Co(III/IV)}$  ions is formed.<sup>94</sup> Due to the electrocatalytic reaction and the oxidization reaction conditions,  $T_d$  Co ions change their coordination to octahedral leading to the reaction zone in the near-surface.

Current–time chronoamperometry measurements of  $\text{ZnCo}_2\text{O}_4$  were also carried out for a period of 10 hours and about 20% decrease in the catalytic activity was observed (Fig. S23†). The overpotential at 10  $\text{mA cm}^{-2}$  obtained after the stability tests was in fact only 40 mV higher than that of the as-prepared  $\text{ZnCo}_2\text{O}_4$  catalyst (Fig. S24†). Moreover, ICP-AES and EDX analyses revealed that  $\sim 30\%$  of Zn was leached from the surface.

It can be considered feasible that Zn leaching enhances the amorphization of the near-surface and increases the specific activity of the Co oxides. Furthermore, the beneficial influence of the presence of hydroxylation in the near-surface and OER activity was recently shown for IrNi oxide model catalysts.<sup>95</sup> Apparently, the activity of  $(\text{Co}_3\text{O}_4)/(\text{ZnO})_6$  is lower than that of  $\text{ZnCo}_2\text{O}_4$  and  $\text{Co}_3\text{O}_4$ , due to the presence of a higher amount of inactive Zn and a lower amount of Co. The results obtained here substantiate the role of metal ions in  $T_d$  and  $O_h$  sites and their structure–activity relationship. In addition to the superior performance of the catalysts, the cost-effective synthetic route as well as large-scale production of the catalysts in a robust way makes this study very appealing.

## Conclusions

A facile, environmentally friendly and cost-effective synthetic route has been applied for the large-scale (multi-gram scale) production of cobalt–zinc oxides as high-performance OER catalysts. The electrochemical OER in alkaline solution displayed enhanced oxygen evolution for  $\text{ZnCo}_2\text{O}_4$  generating lower overpotential at 10  $\text{mA cm}^{-2}$  than that of  $\text{Co}_3\text{O}_4$  and  $(\text{Co}_3\text{O}_4)/(\text{ZnO})_6$ . Interestingly, at 20  $\text{mA cm}^{-2}$  the overpotentials of both  $\text{ZnCo}_2\text{O}_4$  and  $\text{Co}_3\text{O}_4$  were barely increased, demonstrating supreme activity of the catalysts. In addition to the overpotentials, considerably smaller Tafel slopes were acquired



for all materials uncovering the efficient reaction kinetics for the OER.

Since  $\text{ZnCo}_2\text{O}_4$  and  $\text{Co}_3\text{O}_4$  belong to the same structure (spinel) type, insights on the structure–activity relationship and the role of metal ions in  $T_d$  and  $O_h$  sites on the surface could be elucidated in detail by microscopic and spectroscopic techniques. It was discovered that the factors influencing the higher activity of  $\text{ZnCo}_2\text{O}_4$  over  $\text{Co}_3\text{O}_4$  could be directly attributed to a higher fraction of available  $O_h$   $\text{Co}^{3+}$  sites, and to the loss of redox-innocent tetrahedral zinc from the surface of the  $\text{ZnCo}_2\text{O}_4$  catalyst during the OER that virtually provides additional vacancies or defective  $T_d$  sites, or surface restructuring, respectively. On the other hand, the  $\text{Co}_3\text{O}_4$  catalyst is much more stable under electrochemical conditions as the  $T_d$   $\text{Co}^{2+}$  ions in contrast to  $\text{Zn}^{2+}$  change their coordination but remain predominantly in the reaction zone of catalysts. With this approach, not only one can design, modify and fabricate catalysts structurally for the upscaling of the efficient OER but also the catalysts could be used in other numerous fields of renewable energy conversion and storage.

## Acknowledgements

Financial support by the BMBF (L2H project) and the DFG (Cluster of Excellence UniCat) as well as by German Federal Ministry of Education and Research (BMBF) through the projects 'MEOKATS' and 'CO2EKAT' is gratefully acknowledged. Authors would also like to thank Dr Caren Göbel for TEM measurements and Dr Vitaly Gutkin for XPS measurements. We thank the Helmholtz Zentrum Berlin for the allocation of synchrotron radiation beamtime.

## References

- H. Dau, C. Limberg, T. Reier, M. Risch, S. Roggan and P. Strasser, *ChemCatChem*, 2010, **2**, 724.
- I. Katsounaros, S. Cherevko, A. R. Zeradjanin and K. J. J. Mayrhofer, *Angew. Chem., Int. Ed.*, 2014, **53**, 102.
- H. B. Gray, *Nat. Chem.*, 2009, **1**, 112.
- J. R. McKone, N. S. Lewis and H. B. Gray, *Chem. Mater.*, 2013, **26**, 407.
- J. Luo, J.-H. Im, M. T. Mayer, M. Schreier, M. K. Nazeeruddin, N.-G. Park, S. D. Tilley, H. J. Fan and M. Grätzel, *Science*, 2014, **345**, 1593.
- T. J. Meyer, *Nature*, 2008, **451**, 778.
- S. W. Lee, C. Carlton, M. Risch, Y. Surendranath, S. Chen, S. Furutsuki, A. Yamada, D. G. Nocera and Y. Shao-Horn, *J. Am. Chem. Soc.*, 2012, **134**, 16959.
- (a) A. Indra, P. W. Menezes, M. Schwarze and M. Driess, *New J. Chem.*, 2014, **38**, 1942; (b) A. Indra, P. W. Menezes, F. Schuster and M. Driess, *J. Photochem. Photobiol., B*, 2015, **152**, 156.
- P. W. Menezes, A. Indra, D. González-Flores, N. R. Sahraie, I. Zaharieva, M. Schwarze, P. Strasser, H. Dau and M. Driess, *ACS Catal.*, 2015, **5**, 2017.
- P. W. Menezes, A. Indra, O. Levy, K. Kailasam, V. Gutkin, J. Pfrommer and M. Driess, *Chem. Commun.*, 2015, **51**, 5005.
- M. W. Kanan and D. G. Nocera, *Science*, 2008, **321**, 1072.
- D. A. Lutterman, Y. Surendranath and D. G. Nocera, *J. Am. Chem. Soc.*, 2009, **131**, 3838.
- (a) P. W. Menezes, A. Indra, P. Littlewood, M. Schwarze, C. Göbel, R. Schomaecker and M. Driess, *ChemSusChem*, 2014, **7**, 2202; (b) M. Risch, K. A. Stoerzinger, S. Maruyama, W. T. Hong, I. Takeuchi and Y. Shao-Horn, *J. Am. Chem. Soc.*, 2014, **136**, 5229.
- (a) F. Jiao and H. Frei, *Chem. Commun.*, 2010, **46**, 2920; (b) M. Fekete, R. K. Hocking, S. L. Y. Chang, C. Italiano, A. F. Patti, F. Arena and L. Spiccia, *Energy Environ. Sci.*, 2013, **6**, 2222.
- A. Bergmann, I. Zaharieva, H. Dau and P. Strasser, *Energy Environ. Sci.*, 2013, **6**, 2745.
- A. Indra, P. W. Menezes, I. Zaharieva, E. Baktash, J. Pfrommer, M. Schwarze, H. Dau and M. Driess, *Angew. Chem., Int. Ed.*, 2013, **52**, 13206.
- I. Zaharieva, P. Chernev, M. Risch, K. Klingan, M. Kohlhoff, A. Fischer and H. Dau, *Energy Environ. Sci.*, 2012, **5**, 7081.
- A. Indra, P. W. Menezes and M. Driess, *ChemSusChem*, 2015, **8**, 776.
- D. M. Robinson, Y. B. Go, M. Mui, G. Gardner, Z. Zhang, D. Mastrogiovanni, E. Garfunkel, J. Li, M. Greenblatt and G. C. Dismukes, *J. Am. Chem. Soc.*, 2013, **135**, 3494.
- Y. Gorlin, C.-J. Chung, J. D. Benck, D. Nordlund, L. Seitz, T.-C. Weng, D. Sokaras, B. M. Clemens and T. F. Jaramillo, *J. Am. Chem. Soc.*, 2014, **136**, 4920.
- M. M. Najafpour, T. Ehrenberg, M. Wiechen and P. Kurz, *Angew. Chem., Int. Ed.*, 2010, **49**, 2233.
- (a) J. Suntivich, K. J. May, H. A. Gasteiger, J. B. Goodenough and Y. Shao-Horn, *Science*, 2012, **334**, 1383; (b) C. G. Morales-Guio, M. T. Mayer, A. Yella, S. D. Tilley, M. Grätzel and X. Hu, *J. Am. Chem. Soc.*, 2015, **137**, 9927.
- (a) P. W. Menezes, A. Indra, N. R. Sahraie, A. Bergmann, P. Strasser and M. Driess, *ChemSusChem*, 2015, **8**, 164; (b) L.-A. Stern, L. Feng, F. Song and X. Hu, *Energy Environ. Sci.*, 2015, **8**, 2347.
- (a) D. G. Nocera, *Acc. Chem. Res.*, 2012, **45**, 767; (b) F. Song and X. Hu, *J. Am. Chem. Soc.*, 2014, **136**, 16481.
- (a) T. Maiyalagan, K. A. Jarvis, S. Therese, P. J. Ferreira and A. Manthiram, *Nat. Commun.*, 2014, **5**, 3949; (b) H. S. Ahn, J. Yano and T. D. Tilley, *ACS Catal.*, 2015, **5**, 2573.
- (a) Y. Gorlin and T. F. Jaramillo, *J. Am. Chem. Soc.*, 2010, **132**, 13612; (b) H. S. Ahn, J. Yano and T. D. Tilley, *Energy Environ. Sci.*, 2013, **6**, 3080.
- (a) A. Singh and L. Spiccia, *Coord. Chem. Rev.*, 2013, **257**, 2607; (b) M. Wiechen, M. M. Najafpour, S. I. Allakhverdiev and L. Spiccia, *Energy Environ. Sci.*, 2014, **7**, 2203.
- Y. Lee, J. Suntivich, K. J. May, E. E. Perry and Y. Shao-Horn, *J. Phys. Chem. Lett.*, 2012, **3**, 399.
- N. Hong Nhan, H.-S. Oh, T. Reier, E. Willinger, M.-G. Willinger, V. Petkov, D. Teschner and P. Strasser, *Angew. Chem., Int. Ed.*, 2015, **54**, 2975.
- H. N. Nong, L. Gan, E. Willinger, D. Teschner and P. Strasser, *Chem. Sci.*, 2014, **5**, 2955.
- T. Reier, M. Oezaslan and P. Strasser, *ACS Catal.*, 2012, **2**, 1765.

- 32 M. G. Walter, E. L. Warren, J. R. McKone, S. W. Boettcher, Q. Mi, E. A. Santori and N. S. Lewis, *Chem. Rev.*, 2010, **110**, 6446.
- 33 E. Antolini, *ACS Catal.*, 2014, **4**, 1426.
- 34 F. A. Frame, T. K. Townsend, R. L. Chamousis, E. M. Sabio, T. Dittrich, N. D. Browning and F. E. Osterloh, *J. Am. Chem. Soc.*, 2011, **133**, 7264.
- 35 D. Wang, X. Chen, D. G. Evans and W. Yang, *Nanoscale*, 2013, **5**, 5312.
- 36 Y. Liang, Y. Li, H. Wang, J. Zhou, J. Wang, T. Regier and H. Dai, *Nat. Mater.*, 2011, **10**, 780.
- 37 Y. Liang, H. Wang, J. Zhou, Y. Li, J. Wang, T. Regier and H. Dai, *J. Am. Chem. Soc.*, 2012, **134**, 3517.
- 38 X. Cao, C. Jin, F. Lu, Z. Yang, M. Shen and R. Yang, *J. Electrochem. Soc.*, 2014, **161**, H296.
- 39 Y. Yang, H. Fei, G. Ruan, C. Xiang and J. M. Tour, *ACS Nano*, 2014, **8**, 9518.
- 40 D. González-Flores, I. Sanchez, I. Zaharieva, K. Klingan, J. Heidkamp, P. Chernev, P. W. Menezes, M. Driess, H. Dau and M. L. Montero, *Angew. Chem., Int. Ed.*, 2015, **54**, 2472.
- 41 K. Klingan, F. Ringleb, I. Zaharieva, J. Heidkamp, P. Chernev, D. González-Flores, M. Risch, A. Fischer and H. Dau, *ChemSusChem*, 2014, **7**, 1301.
- 42 S. Cobo, J. Heidkamp, P.-A. Jacques, J. Fize, V. Fourmond, L. Guetaz, B. Jousselme, V. Ivanova, H. Dau, S. Palacin, M. Fontecave and V. Artero, *Nat. Mater.*, 2012, **11**, 802.
- 43 F. Song and X. Hu, *J. Am. Chem. Soc.*, 2014, **136**, 16481.
- 44 X. Deng and H. Tuysuz, *ACS Catal.*, 2014, **4**, 3701.
- 45 J. D. Blakemore, H. B. Gray, J. R. Winkler and A. M. Mueller, *ACS Catal.*, 2013, **3**, 2497.
- 46 A. Indra, P. W. Menezes, N. R. Sahraie, A. Bergmann, C. Das, M. Tallarida, D. Schmeisser, P. Strasser and M. Driess, *J. Am. Chem. Soc.*, 2014, **136**, 17530.
- 47 Q. Zhang, Z. D. Wei, C. Liu, X. Liu, X. Q. Qi, S. G. Chen, W. Ding, Y. Ma, F. Shi and Y. M. Zhou, *Int. J. Hydrogen Energy*, 2012, **37**, 822.
- 48 J. Rosen, G. S. Hutchings and F. Jiao, *J. Catal.*, 2014, **310**, 2.
- 49 S. Yusuf and F. Jiao, *ACS Catal.*, 2012, **2**, 2753.
- 50 M. S. Burke, M. G. Kast, L. Trotochaud, A. M. Smith and S. W. Boettcher, *J. Am. Chem. Soc.*, 2015, **137**, 3638.
- 51 B. Chi, J. B. Li, X. Z. Yang, H. Lin and N. Wang, *Electrochim. Acta*, 2005, **50**, 2059.
- 52 X. Liu, Z. Chang, L. Luo, T. Xu, X. Lei, J. Liu and X. Sun, *Chem. Mater.*, 2014, **26**, 1889.
- 53 (a) J. Pfrommer, M. Lublow, A. Azarpira, C. Göbel, M. Lücke, A. Steigert, M. Pogrzeba, P. W. Menezes, A. Fischer, T. Schedel-Niedrig and M. Driess, *Angew. Chem., Int. Ed.*, 2014, **53**, 5183; (b) F. Rong, J. Zhao, P. Su, Y. Yao, M. Li, Q. Yang and C. Li, *J. Mater. Chem. A*, 2015, **3**, 4010.
- 54 (a) T. W. Kim, M. A. Woo, M. Regis and K.-S. Choi, *J. Phys. Chem. Lett.*, 2014, **5**, 2370; (b) Y. Li, L. Zhang, X. Xiang, D. Yan and F. Li, *J. Mater. Chem. A*, 2014, **2**, 13250.
- 55 W. L. Roth, *J. Phys. Chem. Solids*, 1964, **25**, 1.
- 56 K. Krezhov and P. Konstantinov, *J. Phys.: Condens. Matter*, 1993, **5**, 9287.
- 57 S. C. Abrahams and J. L. Bernstein, *Acta Crystallogr., Sect. B: Struct. Crystallogr. Cryst. Chem.*, 1969, **25**, 1233.
- 58 M. Oku and K. Hirokawa, *J. Electron Spectrosc. Relat. Phenom.*, 1976, **8**, 475.
- 59 W. Song, A. S. Poyraz, Y. Meng, Z. Ren, S.-Y. Chen and S. L. Suib, *Chem. Mater.*, 2014, **26**, 4629.
- 60 L. L. Hu, B. H. Qu, C. C. Li, Y. J. Chen, L. Mei, D. N. Lei, L. B. Chen, Q. H. Li and T. H. Wang, *J. Mater. Chem. A*, 2013, **1**, 5596.
- 61 T. Baird, K. C. Campbell, P. J. Holliman, R. W. Hoyle, D. Stirling, B. P. Williams and M. Morris, *J. Mater. Chem.*, 1997, **7**, 319.
- 62 J. Li, J. Wang, X. Liang, Z. Zhang, H. Liu, Y. Qian and S. Xiong, *ACS Appl. Mater. Interfaces*, 2014, **6**, 24.
- 63 B. J. Tan, K. J. Klabunde and P. M. A. Sherwood, *J. Am. Chem. Soc.*, 1991, **113**, 855.
- 64 S. Ma, L. Sun, L. Cong, X. Gao, C. Yao, X. Guo, L. Tai, P. Mei, Y. Zeng, H. Xie and R. Wang, *J. Phys. Chem. C*, 2013, **117**, 25890.
- 65 J. Y. Sa, K. Kwon, J. Y. Cheon, F. Kleitz and S. H. Joo, *J. Mater. Chem. A*, 2013, **1**, 9992.
- 66 J. A. Koza, Z. He, A. S. Miller and J. A. Switzer, *Chem. Mater.*, 2012, **24**, 3567.
- 67 T. Grewe, X. Deng and H. Tueysuez, *Chem. Mater.*, 2014, **26**, 3162.
- 68 M. Grzelczak, J. Zhang, J. Pfrommer, J. Hartmann, M. Driess, M. Antonietti and X. Wang, *ACS Catal.*, 2013, **3**, 383.
- 69 C. C. L. McCrory, S. Jung, I. M. Ferrer, S. M. Chatman, J. C. Peters and T. F. Jaramillo, *J. Am. Chem. Soc.*, 2015, **137**, 4347.
- 70 C. C. L. McCrory, S. Jung, J. C. Peters and T. F. Jaramillo, *J. Am. Chem. Soc.*, 2014, **135**, 16977.
- 71 J. Jiang, J. P. Liu, X. T. Huang, Y. Y. Li, R. M. Ding, X. X. Ji, Y. Y. Hu, Q. B. Chi and Z. H. Zhu, *Cryst. Growth Des.*, 2010, **10**, 70.
- 72 G. Spinolo, S. Ardizzone and S. Trasatti, *J. Electroanal. Chem.*, 1997, **423**, 49.
- 73 S. Palmas, F. Ferrara, A. Vacca, M. Mascia and A. M. Polcaro, *Electrochim. Acta*, 2007, **53**, 400.
- 74 E. B. Castro and C. A. Gervasi, *Int. J. Hydrogen Energy*, 2000, **25**, 1163.
- 75 J. B. Gerken, J. G. McAlpin, J. Y. C. Chen, M. L. Rigsby, W. H. Casey, R. D. Britt and S. S. Stahl, *J. Am. Chem. Soc.*, 2011, **133**, 14431.
- 76 E. B. Castro, C. A. Gervasi and J. R. Vilche, *J. Appl. Electrochem.*, 1998, **28**, 835.
- 77 D. R. Rolison, P. L. Hagans, K. E. Swider and J. W. Long, *Langmuir*, 1999, **15**, 774.
- 78 J. O. Bockris and T. Otagawa, *J. Phys. Chem.*, 1983, **87**, 2960.
- 79 X. Zou, A. Goswami and T. Asefa, *J. Am. Chem. Soc.*, 2013, **135**, 17242.
- 80 (a) E. Rios, P. Chartier and J. L. Gautier, *Solid State Sci.*, 1999, **1**, 267; (b) U. Maitra, B. S. Naidu, A. Govindaraj and C. N. R. Rao, *Proc. Natl. Acad. Sci. U. S. A.*, 2013, **110**, 11704.
- 81 E. Rios, H. Reyes, J. Ortiz and J. L. Gautier, *Electrochim. Acta*, 2005, **50**, 2705.



- 82 M. Hamdani, R. N. Singh and P. Chartier, *Int. J. Electrochem. Sci.*, 2010, **5**, 556.
- 83 Y. Li, P. Hasin and Y. Wu, *Adv. Mater.*, 2010, **22**, 1926.
- 84 B. S. Yeo and A. T. Bell, *J. Am. Chem. Soc.*, 2011, **133**, 5587.
- 85 J. G. McAlpin, Y. Surendranath, M. Dinca, T. A. Stich, S. A. Stoian, W. H. Casey, D. G. Nocera and R. D. Britt, *J. Am. Chem. Soc.*, 2010, **132**, 6882.
- 86 M. Risch, K. Klingan, F. Ringleb, P. Chernev, I. Zaharieva, A. Fischer and H. Dau, *ChemSusChem*, 2012, **5**, 542.
- 87 M. Risch, F. Ringleb, M. Kohlhoff, P. Bogdanoff, P. Chernev, I. Zaharieva and H. Dau, *Energy Environ. Sci.*, 2015, **8**, 661.
- 88 A. Kuzmin, S. Larcheri and F. Rocca, *J. Phys.*, 2007, **93**, 012045.
- 89 O. Sivr and F. Rocca, *J. Phys.: Condens. Matter*, 2011, **23**, 6.
- 90 M. Risch, A. Grimaud, K. J. May, K. A. Stoerzinger, T. J. Chen, A. N. Mansour and Y. Shao-Horn, *J. Phys. Chem. C*, 2013, **117**, 8628.
- 91 M. Risch, V. Khare, I. Zaharieva, L. Gerencser, P. Chernev and H. Dau, *J. Am. Chem. Soc.*, 2009, **131**, 6936.
- 92 T. Reier, D. Teschner, T. Lunkenbein, A. Bergmann, S. Selve, R. Kraehnert, R. Schlögl and P. Strasser, *J. Electrochem. Soc.*, 2014, **161**, F876.
- 93 M. Bernicke, E. Ortel, T. Reier, A. Bergmann, J. Ferreira de Araujo, P. Strasser and R. Kraehnert, *ChemSusChem*, 2015, **8**, 1908.
- 94 A. Bergmann, E. Martinez-Moreno, D. Teschner, P. Chernev, M. Gliech, J. F. de Araújo, T. Reier, H. Dau and P. Strasser, *Nat. Commun.*, 2015, **6**, 8625.
- 95 T. Reier, Z. Pawolek, S. Cherevko, M. Bruns, T. Jones, D. Teschner, S. Selve, A. Bergmann, H. N. Nong, R. Schlögl, K. J. J. Mayrhofer and P. Strasser, *J. Am. Chem. Soc.*, 2015, **137**, 13031.